Interactions of Water with Pyridine and Benzene Studied by TOF-SIMS

Ryutaro Souda*

Advanced Materials Laboratory, National Institute for Materials Science, 1-1 Namiki, Tsukuba, Ibaraki 305-0044, Japan

Received: July 11, 2003; In Final Form: November 7, 2003

TOF-SIMS is used to characterize the weak intermolecular interactions between heavy water and aromatic molecules such as benzene and pyridine in order to gain insight into solvation. The D_2O molecules dissolve in the thin-layer bulk of pyridine above 110 K due to the formation of hydrogen bonds, but they are hardly incorporated in the benzene layer. The benzene molecules dissolve in the D_2O layer via hydrophobic hydration for $T > 120$ K, whereas the pyridine remains on the D_2O layer up to the desorption temperature of 180 K. Pyridine forms hydrogen bonds with the D_2O, but no indication of hydrophobic hydration is observed except at temperatures around 150 K where the mobility of the D_2O molecules would be increased due to the phase transition to the cubic ice. From the comparison of the hydration patterns between pyridine and benzene, it is suggested that hydrophobic hydration tends to be quenched on the surface if the hydrophilic hydration coexists. This is because the hydrophobic interaction is energetically a minor process compared to hydrophilic interactions, so that the water structure is determined by the normal O−D···N and O−D···O hydrogen bonds.

1. Introduction

The interaction between hydrocarbons and water is one of the most important forces in nature. It plays a major role in the conformation of proteins and the formation of micelles and biological membranes. Benzene and pyridine are prototypical aromatic molecules and their structures are incorporated in many biologically important molecules. Aromatic−water interactions present a special challenge to the experiment and theory in terms of the role of the conjugated π system. The in-plane interactions of water with benzene would be hydrophobic, but the π electrons should lead to hydrophilic out-of-plane interactions due to their polarizability.[1] In addition, pyridine undergoes hydrophilic hydration at the nitrogen-atom site. Thus, insight into hydrophilic and hydrophobic hydration would be obtained by comparing the hydration patterns between benzene and pyridine. Our current understanding of aromatic−water interactions mainly relies on experiments for small gas-phase clusters,[2−5] but more insight into the hydration phenomenon should be obtained from adsorption systems on the water-ice surface. Indeed, knowledge of intermolecular interactions on the water-ice surface and the transport of adsorbed molecules into the bulk is of particular importance for understanding the mechanism of hydration at the molecular level. One of the most powerful spectroscopic probes of hydration has been provided by infrared absorption spectroscopy.[6] However, the disadvantage of this method is its relatively poor surface sensitivity. Electron spectroscopic techniques have been applied to the analysis of molecular adsorption on the water-ice surface,[7] but they sometimes encounter difficulties in characterizing highly insulating molecular-solid surfaces, as well as weak intermolecular interactions via the van der Waals force and hydrogen bonding. Very recently, it was demonstrated that hydration and H/D exchange of protic molecules, such as NH_3 and CH_3OH, can be analyzed successfully using time-of-flight secondary ion mass spectrometry (TOF-SIMS).[8,9] So far, molecular solid surfaces have been studied extensively by using static SIMS.[10−12] Since the secondary ions are sputtered basically from the topmost surface layer, SIMS is regarded as one of the most surface-sensitive techniques. A more important aspect in SIMS is that protonated molecular ions are created as a consequence of proton-transfer reactions during collisions of neutral molecules (e.g., $2H_2O \rightarrow H_3O^+ + OH^-$), which enables us to explore the local conformation of hydrogen-bonded molecules on the surface.

This paper will report on solvation patterns found in the systems composed of C_6H_6, C_5H_5N, and D_2O molecules on the basis of temperature evolutions of the TOF-SIMS cation yields, as well as the temperature-programmed desorption (TPD) and X-ray photoelectron spectroscopy (XPS). The transport properties of molecules from the surface into the bulk will be discussed in terms of the hydrophilic and hydrophobic modes of solvation.

2. Experiment

The experiments were carried out in an ultrahigh-vacuum chamber (base pressure of 1×10^{-10} mbar) equipped with facilities for standard surface characterization, such as a quadrupole mass spectrometer, an X-ray source, and a hemispherical electrostatic analyzer. The He^+ ions, produced in an electron-impact-type ion source, were chopped by an electrostatic deflector into pulses with width of 200 ns and frequency of 40 kHz. The TOF-SIMS measurements were made in such a manner that the sample, floated with a bias voltage of +500 eV, was irradiated with a primary He^+ beam of 2 keV through a grounded stainless steel mesh placed 4 mm above the sample surface (the ion impact energy was 1.5 keV), and the positive ions extracted into the field-free region of the TOF tube were detected with a channel electron multiplier. To minimize charging and damage of a surface, a pulsed He^+ beam with a low incident flux (0.2 nA/cm^2) was used. The substrate was a polycrystalline Ni sheet mounted on a sample holder cooled to 15 K by means of a closed-cycle He refrigerator. The surface was cleaned by annealing around 1200 K. The D_2O, C_6H_6, and C_5H_5N molecules were admitted into the vacuum chamber

* E-mail: SOUDA.Ryutaro@nims.go.jp.

10.1021/jp035996p CCC: $27.50
Published on Web 12/10/2003

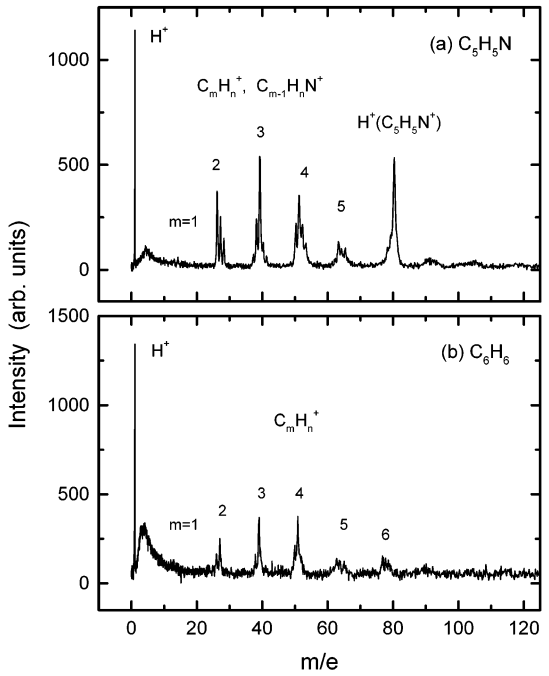

Figure 1. TOF−SIMS spectra of positive ions from thin layers (20 ML) of (a) C_5H_5N and (b) C_6H_6 deposited at 15 K. The measurements were made by bombardment of 1.5-keV He^+ ions.

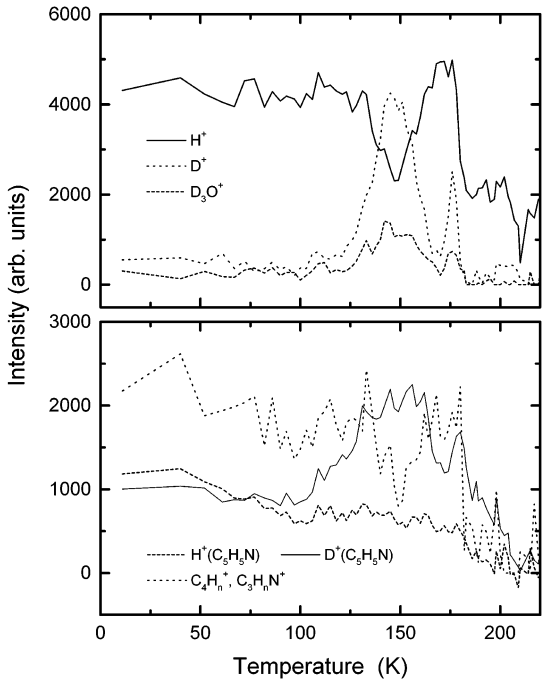

Figure 2. Evolutions of typical secondary-ion yields from the pyridine (1 ML)-adsorbed D_2O layer (50 ML) as a function of temperature. The molecules were deposited at temperature of 15 K, and the surfaces were irradiated with a He^+ beam of 1.5 keV.

through independent variable-leak valves. The D_2O molecules were deposited on the Ni substrate at temperature of 15 K. The morphology of water ice thus grown is known to be dependent upon the substrate temperature: the cubic crystalline ice phase exists above the temperature of 140 K, below which amorphous solid water is grown. The water films grown below 90 K have porosity and some molecules, such as N_2 and CO, can be incorporated in the pores.[13] In the present study, however, the adsorbed C_6H_6 and C_5H_5N molecules were not incorporated in the inner pores of D_2O ice. One-monolayer (1 ML) coverage of the adsorbed molecules was determined from the decay curve of the sputtered ion yields from the substrate molecules as a function of exposure, and the film thickness was estimated on the basis of this value. The temperature evolutions of the secondary-ion yields were measured by collecting the TOF-SIMS spectra at time intervals of 30 s for a temperature increasing rate of about 0.1 K s^{-1} ($T > 100$ K).

3. Experimental Results

Figure 1 shows TOF-SIMS spectra of positive ions from thin layers of (a) C_5H_5N and (b) C_6H_6 molecules, which are deposited with a thickness of 20 ML at a substrate temperature of 15 K. The primary secondary ion species are H^+ and fragment ions, such as $C_mH_n^+$ ($m = 1-6$ for benzene) and $C_mH_n^+$ or $C_{m-1}H_nN^+$ ($m = 1-5$ for pyridine). The cracking patterns of secondary ions exhibit quite similar profiles between the C_5H_5N and C_6H_6 molecules. In this paper, we do not discuss details of the fragment-ion formation. It should be noted that the protonated molecular ion, $H^+(C_5H_5N)$, is sputtered from pyridine considerably whereas the yield of protonated benzene is negligibly small. This type of molecular ions is known to be sputtered from hydrogen-bonded systems, such as H_2O, NH_3, HCOOH, and CH_3OH, as a result of the proton-transfer reaction during collisions.[8,9] Although pyridine is aprotic with no ordinary hydrogen bonds, the $H^+(C_5H_5N)$ ion is created due to the donation of a proton from the C−H group during intermolecular collisions, suggesting that the C−H group acts as a proton donor in "nonstandard" hydrogen bonding.[14,15] A broad structure starting at the leading edge ($m/e = 0$) is not due to the secondary ions but is caused by the energetic He^0 atoms backscattered from the surface.

Shown in Figure 2 are evolutions of typical secondary ion yields from C_5H_5N (1 ML) adsorbed on the D_2O-ice surface (50 ML) as a function of temperature. The data for some fragment-ion species are noisy because of the high instrumental backgrounds, but the evolution curves of secondary ions exhibit some characteristic features occurring at specific temperatures. The D^+-attached pyridine is sputtered considerably and it becomes predominant over the H^+-attached pyridine for $T >$ 100 K. The $D^+(C_5H_5N)$ yield shows two peaks around 150 and 180 K. It should be noticed that the evolution of the $D^+(C_5H_5N)$ yield is quite similar to that of the D^+ and D_3O^+ yields. On the other hand, the yields of H^+ and fragment ions from pyridine exhibit a dip around 150 K. The deuterated pyridine is created during collisions with the D_2O molecules via the deuteron-transfer reaction, $D_2O + C_5H_5N \rightarrow OD^- + D^+(C_5H_5N)$, so that its yield should be related to the number of the pyridine molecules interacting with the D_2O molecules. The D_2O layer desorbs, together with the C_5H_5N molecules, above 180 K, as revealed from the sudden drops of the secondary-ion yields as well as the steep evolution of Ni^+ sputtered from the substrate (not shown).

In Figure 3 are shown the temperature evolutions of secondary ions from the C_6H_6 molecule (1 ML) adsorbed on the D_2O layer (50 ML). The molecules were deposited at 15 K. The C_6H_6 molecules disappear from the surface above 120 K and the surface is finally covered with the pure D_2O layer. Probably, this result is described by the incorporation of the C_6H_6 molecules in the D_2O layer. As mentioned earlier, the morphology of the water ice depends on the temperature. The mixing of molecules would be promoted on the rougher D_2O-ice surface prepared at 15 K, since a larger number of the C_6H_6 molecules can make contact with the D_2O molecules, thereby facilitating the hydration when the temperature is increased. To confirm

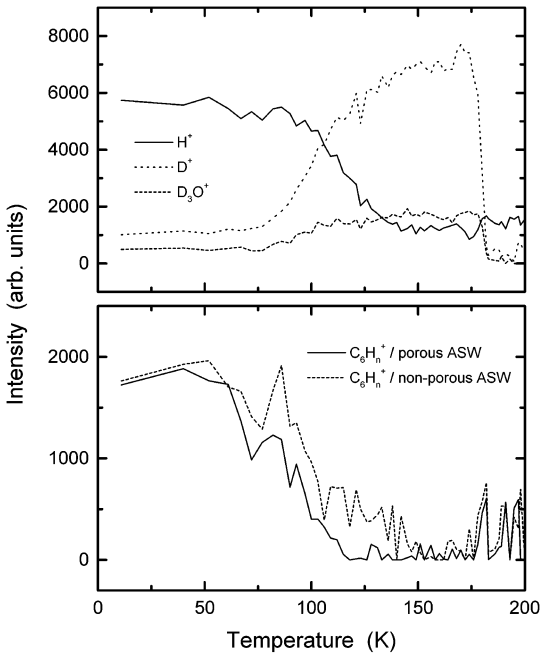

Figure 3. Evolutions of typical secondary-ion yields from the benzene (1 ML)-adsorbed D_2O layer (50 ML) as a function of temperature. The molecules were deposited at a temperature of 15 K. In the bottom panel, the $C_6H_n^+$ yield from benzene adsorbed on the nonporous amorphous solid water (ASW) is shown by the broken line in comparison with that on the porous amorphous solid water (solid line). The resonant-like features in the two $C_6H_n^+$ spectra at $T > 175$ K are false, due to the instrumental background.

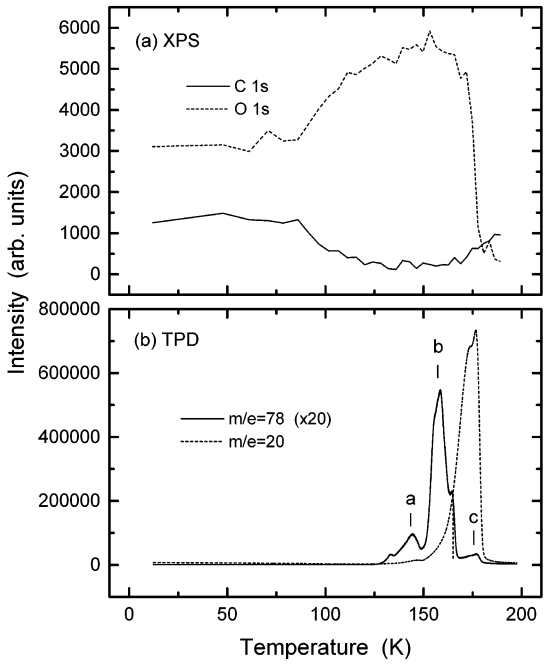

Figure 4. (a) Evolutions of C 1s and O 1s peak intensities in the XPS spectra from the benzene (1 ML)-adsorbed D_2O layer (50 ML) as a function of temperature. The surface was excited with unmonochromatized Mg Kα irradiation (1253.6 eV), and electrons emitted through 30° with respect to the surface normal were detected. (b) TPD spectra of C_6H_6 ($m/e = 78$) and D_2O ($m/e = 20$) from the benzene (1 ML) adsorbed D_2O layer (50 ML).

such a morphological effect of the D_2O ice on the hydration, the C_6H_6 molecules were deposited on the surface of nonporous amorphous solid water (ASW) prepared at 100 K. The evolution curve of the $C_6H_n^+$ ion from the ASW surface is typically shown in Figure 3. As expected, the ion yield decays more gradually on the ASW than on the porous-ASW, but the hydration of benzene occurs finally irrespective of the roughness of the water-ice surface.

In Figure 3, it might be presumed that the decay of the $C_6H_n^+$ ion above 120 K is caused by desorption of the C_6H_6 molecules rather than hydration. To deny such a possibility, complementary XPS and TPD measurements were performed for porous-ASW under the same condition as in TOF-SIMS. The results are shown in Figure 4. In XPS, essentially the same results as in TOF-SIMS were obtained: the C 1s peak from the C_6H_6 molecule decays considerably above 80 K and the O 1s peak from D_2O evolves. This phenomenon cannot be ascribed to desorption of the C_6H_6 molecules since noticeable desorption of the C_6H_6 molecule ($m/e = 78$) occurs only above 130 K as revealed from the TPD measurement. The characteristic three peaks denoted as a−c, together with small satellite peaks, are clearly observed in TPD. It is known that quite similar peaks, α_1, α_2, and α_3, occur at around 167, 143, and 153 K, respectively, in the TPD spectra of benzene from metal substrates.[16−18] The α_1 phase (corresponding to peak c) has been ascribed to the first physisorbed monolayer lying on the closely packed, uniformly chemisorbed C_6H_6 layer. Further adsorption leads to the α_2 phase which has been assigned to a denser monolayer with benzene molecules standing edge-on. Finally, bulklike, a randomly oriented benzene multilayer (α_3) grows at higher coverage. In the present experiment, the origins of peaks a−c might be different from those observed for the metal substrate, but the dominance of peak b (corresponding to peak α_3) at such small coverage as 1 ML may be remarkable. This result may suggest that 3-D clusters of benzene are formed in the D_2O matrix during the heating process, as inferred from the fact that no evolutions of the C 1s peak in XPS and the $C_6H_n^+$ ion in SIMS occur at this temperature. Note that peak a is accompanied by a small hump for D_2O desorption and that the main desorption peak of the D_2O molecules occurs at the same temperature as for peak c. Moreover, the onset of peak b corresponds well to that of the main peak of D_2O desorption. All these facts indicate the presence of some water−benzene interactions during desorption. It is known that desorption of some hydrophobic molecules, such as N_2 and CCl_4, embedded in the ASW layer is delayed considerably[19,20] and occurs abruptly at the crystallization temperature of ASW (the molecular volcano).[21] In the present TPD experiment, however, no shift of the desorption temperature is observed at all relative to that for the pure C_6H_6 layer, suggesting that the benzene is not buried deeply, but may be just below the surface of water ice.

In Figure 5 are shown the yields of some secondary ions sputtered from the D_2O molecule (1 ML) adsorbed on the C_5H_5N layer (20 ML) as a function of temperature. The D^+ and D_3O^+ ions decay in intensity with increasing temperature and disappear completely from the surface above 115 K. The yields of the fragment ions, as well as D^+- and H^+-attached molecular ions, form a peak at this temperature. The $D^+(C_5H_5N)$ yield remains considerably up to 140 K and exhibits a small dip around 155 K where the $H^+(C_5H_5N)$ yield is increased alternatively. All these behaviors should be related to the change in the structure of the pyridine layer as a consequence of the solvation of the adsorbed D_2O molecules. The C_5H_5N layer evaporates above 175 K. The peak in the H^+ yield around 50 K would be caused by segregation/desorption of impurity molecules dissolved in the pyridine layer during the sample preparation. The impurities cannot be identified in Figure 1 since they are incorporated in the thin-layer bulk with a relatively small concentration. The $m/e = 14$ species, though small in intensity, evolves concomi-

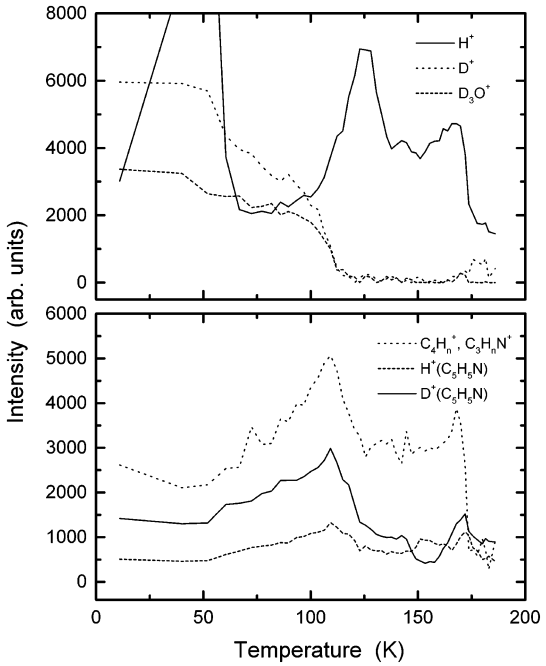

Figure 5. Temperature evolutions of some secondary ion yields from the D_2O-adsorbed pyridine layer. The D_2O molecules (1.0 ML) were deposited on the C_5H_5N layer (20 ML) at temperature of 15 K.

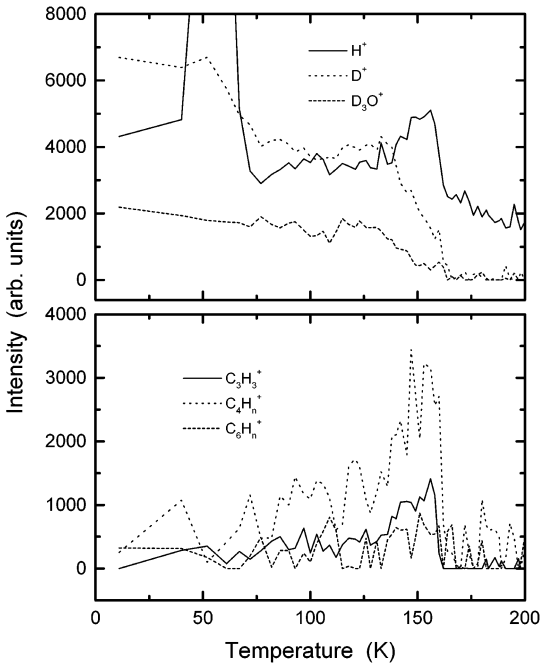

Figure 6. Temperature evolutions of some secondary-ion yields from the D_2O-adsorbed benzene layer. The D_2O molecules (1.0 ML) were deposited on the C_6H_6 layer (20 ML) at a temperature of 15 K.

tantly with the H^+ ion in this temperature regime, suggesting that the segregated N_2 impurities play a role. In this respect, the sputtered H^+ yield from H_2O and CH_4 molecules adsorbed on the surfaces of some molecular solids, such as N_2, CO, and Ar, is known to be enhanced considerably due to the formation of a complex.[22,23]

The temperature evolutions of secondary ions from D_2O (1 ML) adsorbed on the C_6H_6 layer (20 ML) are shown in Figure 6. The D_2O molecules are hardly incorporated in the benzene layer in comparison with the pyridine layer. The D^+ and D_3O^+ yields (the H^+ and $C_mH_n^+$ yields) decrease (increase) above 140 K due to the morphological change or the incorporation in part of the adsorbed D_2O molecules. The C_6H_6 layer evaporates at 160 K together with the D_2O molecules. The enhanced H^+ yield around 50 K is caused by the segregation of the impurity N_2 molecules to the C_6H_6 surface. The evaporation temperatures of multilayer water (180 K), benzene (160 K), and pyridine (175 K) observed in the present experiment are in good agreement with the typical desorption temperatures of these molecules: e.g., desorption of benzene from Pt(111) occurs at 175 K[24] and the desorption of pyridine from Ag(110) at 168 K.[25]

4. Discussion

4.1. Benzene−Water Interactions. The immiscibility of benzene in liquid water indicates that the benzene−water interaction should be hydrophobic. In the present experiment, however, it is found that the benzene molecule dissolves in the water ice at cryogenic temperatures. The origin of this effect may be explained in terms of the hydrophobic hydration. At low temperatures, hydrophobicity has been explained by the entropic changes of the Gibbs free energy due to the formation of cage structures of the water molecules around the guest molecules, though the nature of hydrophobic hydration is still poorly understood. Recent experimental and theoretical studies have presented evidence for the existence of C−H···O hydrogen bonds under certain conditions.[14,15,26−31] The nature of such nonstandard hydrogen bonds has been attributed primarily to electrostatic interactions,[27] but it is recently claimed that C−H···O interactions can be categorized as true hydrogen bonds though they are weaker due to the lesser proton donor ability of C−H as compared to that of O−H.[14,15] Moreover, the ability of a C−H bond to act as a hydrogen-bond donor is known to increase in the order $C(sp^3)$, $C(sp^2)$, and C(sp).[32] On the other hand, the role of the π cloud of benzene in the formation of hydrogen bonds with water has been discussed theoretically,[1] and the value of the binding energy of the $C_6H_6-H_2O$ complex is calculated as 3.9 kcal/mol. The structures of $C_6H_6-(H_2O)_n$ clusters have also been investigated on the basis of the size-specific infrared spectra and resonant two-photon ionization.[2−5] The most likely structure is such that one of the water molecules sits above the aromatic ring with oxygen pointed away from the benzene center of mass and one of the water hydrogen is oriented toward the ring. No indication of the C−H···O hydrogen bond has been reported from the structural studies of the $C_6H_6-(H_2O)_n$ clusters, suggesting that such interactions (binding energy < 1 kcal/mol[33]) have a minor effect on the water-structure formation around benzene. In the condensed phase, however, such a weak hydrogen bond may also play a role in the hydration of the benzene molecules.

In contrast to the benzene-adsorbed D_2O film, the D_2O molecules adsorbed on the C_6H_6 layer are hardly incorporated in the bulk by increasing temperature up to 160 K. In order for solvation to occur, the interactions to separate adsorbates by a substrate molecule should dominate over the contact interactions of the adsorbates. Probably, the adsorbed D_2O molecules favor structures involving an O−D···O hydrogen-bonding network rather than the formation of the $(C_6H_6)_n-D_2O$ complex, as inferred from that the binding energy for the water−benzene interaction is about 20% weaker than the water−water interaction.[1]

4.2. Pyridine−Water Interactions. One of the characteristic features seen in Figure 1 is that the $H^+(C_5H_5N)$ ion is sputtered considerably from pyridine. The protonated molecular ions are not simply caused by the association of the H^+ ion with the molecules during sputtering processes as evidenced by the fact that the evolution curves of these two ions are completely

different from each other.[8,9] As mentioned above, the ability of the C−H bond to donate a proton is increased with increasing number of π electrons. Therefore, the $H^+(C_5H_5N)$ ion would be created during collisions of the C_5H_5N molecules due to the proton-transfer reaction: C−H···N → C^-···H^+−N.

It is of particular interest that the hydration pattern of pyridine is completely different from that of benzene. It might be presumed that the formation of the O−D···N hydrogen bonding, as well as the nonstandard hydrogen bonding caused by the π cloud or the C−H···N contact, would facilitate the hydration of pyridine. In reality, however, the incorporation of pyridine in the D_2O layer hardly occurs as seen in Figure 2, though the hydrophilic hydration takes place as evidenced by the emission of the $D^+(C_5H_5N)$ ion. From the comparison of the hydration patterns between benzene and pyridine, it is suggested that the hydrophobic hydration competes with the hydrophilic hydration for the adsorption systems. The hydrophobic hydration, caused by the nonstandard hydrogen bonding, may play only a secondary role in the structure formation of water molecules in comparison to the standard O−D···O and O−D···N hydrogen bonding. Because of the predominance of the hydrophilic hydration, therefore, the formation of the cage structure of the water molecules around the hydrophobic part of the pyridine molecule may be disturbed, resulting in the exclusion of the hydrophobic groups from the hydrogen-bonded network of bulk water molecules. The same phenomenon was observed in the hydration patterns of the other molecules, such as NH_3, CH_3NH_2, and CH_3OH, adsorbed on the D_2O layer:[8,9] the NH_3 molecule tends to be incorporated in the thin-layer bulk of water above 140 K whereas the CH_3NH_2 and CH_3OH molecules stand on the surface with the hydrophobic CH_3 end toward the vacuum.

The occurrence of hydrophilic and hydrophobic modes of hydration can be explored from the comparison of the evolution curves between the H^+- or D^+-attached molecular ions and the fragment ions: the former provides us information about the formation of the hydrogen bonds whereas the latter is basically related to the number of the molecules existing on the outermost surface layer or their orientations. In Figure 2, the $D^+(C_5H_5N)$ yield is enhanced relative to the $H^+(C_5H_5N)$ yield for 100 K < T < 180 K due to the formation of hydrogen bonds between the C_5H_5N and D_2O molecules. The peak in the yield of the D^+-attached pyridine around 150 K shows that the hydrophilic hydration is promoted due to the emergence of the D_2O molecules at the topmost surface layer. Most of the D_2O molecules once emerged on the surface disappear around 170 K and evolve again at the desorption temperature. The evolution of the D^+ and D_3O^+ ions, together with the D^+-attached molecular ions, around 150 K is characteristic of the hydration of the C_5H_5N molecule and is not observed for that of the CH_3NH_2 and CH_3OH molecules. Probably, this phenomenon is related to the hydrophobic hydration, which originates from the nonstandard hydrogen bonds between the O−D group of heavy water and the π cloud of pyridine.

For the D_2O adsorption on the pyridine layer (Figure 5), the C_5H_5N molecule forms the O−D···N hydrogen bond considerably even at 15 K as inferred from the high yield of $D^+(C_5H_5N)$ relative to $H^+(C_5H_5N)$. The presence of the D_3O^+ ion shows that the islands or clusters of hydrogen-bonded D_2O molecules coexist on the surface. The yields of the $D^+(C_5H_5N)$ and fragment ions (the D^+ and D_3O^+ ions) increase (decrease) by increasing temperatures up to 110 K. This is simply explicable in terms of the incorporation of the adsorbed D_2O molecules in the thin-layer bulk of pyridine. The invariance of the relative yields between $C_mH_n^+$ (or $C_{m-1}H_nN^+$), $H^+(C_5H_5N)$, and $D^+(C_5H_5N)$ ions in this temperature regime shows that the O−D···N hydrogen bonding is basically completed at 15 K, providing a contrast to the thermally activated behavior of the O−D···N bond formation seen in Figure 2. After the D_2O molecule disappears from the surface, the yields of fragment and molecular ions decrease, whereas the H^+ yield increases and forms a peak at 125 K. This phenomenon is not completely understood but it may be related to the change in the orientation of the pyridine molecules by sticking the hydrophobic part of the aromatic ring out toward the vacuum side. After the complete disappearance of the hydrogen-bonded D_2O molecules from the surface above 115 K, there still exist the D_2O molecules forming the hydrogen bonds with the C_5H_5N molecules, as evidenced by the predominance of $D^+(C_5H_5N)$ over $H^+(C_5H_5N)$. Such D_2O molecules are hardly detected as the D^+ and D_3O^+ ions, respectively, since they are emitted from the dangling O−D bond and the O−D···O hydrogen-bonded D_2O clusters. The D_2O molecules bonded to C_5H_5N diffuse into the bulk between 140 and 160 K as inferred from the dip in the $D^+(C_5H_5N)$ yield and the enhancement of the $H^+(C_5H_5N)$ yield.

The critical temperatures seem to exist around 140−150 K for hydration of pyridine and 110 K for solvation of D_2O by pyridine. The surface of water ice is a complex disordered system, so that a greater molecular mobility is expected than that of bulk water ice. In fact, it is well-known that the water-ice surface is so soft that the surface structure analysis by low-energy electron diffraction[34] and helium atom scattering[35] is difficult at temperatures above 90−125 K. To the best of my knowledge, however, no direct experimental evidence has so far been presented regarding the facile surface diffusion of water molecules at $T \sim 110$ K except for the D_2O adsorption on pyridine (Figure 5) and methanol.[9] Probably, this phenomenon is characteristic of the surfaces of hydrophobic and amphiphilic molecules, where the water molecules can diffuse for a long distance with a small activation energy until the hydrogen bonds are formed finally. It is known that the isotope exchange in the H_2O/D_2O, NH_3/D_2O, and CH_3OH/D_2O systems is promoted above the temperature around 140 K.[8,9,36−38] The nature of ASW above the glass transition temperature (136 K) is still controversial,[36−42] but such a common feature should be ascribed to some propensity inherent in water. Although no conclusive evidence for the liquid phase of the water-ice surface has been presented below 200 K,[39] the ASW may transform to a metastable liquid phase before crystallization near 160 K.[40,41] The transition of water into viscous liquid, coexisting with the cubic ice, has also been suggested at a critical temperature of 140 K.[42] In any case, the water molecules should have high mobility not only on the surface but also in the bulk around this temperature. The evolution of the D^+ and D_3O^+ yields at 140 K as seen in Figure 2 would be induced by such mobile D_2O molecules formed on the surface, resulting in the enhancement not only of the hydrophilic hydration but also of the hydrophobic hydration of pyridine. In Figure 4, moreover, desorption of the C_6H_6 molecule occurs most remarkably above 150 K (peak b in the TPD spectrum). This phenomenon may be caused by the decomposition of the hydrated benzene above the phase-transition temperature, resulting in the direct desorption or the 3-D cluster formation of the C_6H_6 molecules.

5. Conclusion

The intermolecular interactions between aromatic molecules, such as C_6H_6 and C_5H_5N, and D_2O have been investigated at cryogenic temperatures in order to gain more insight in the

solvation phenomena. In the TOF-SIMS spectra, the protonated (deuterated) C_5H_5N molecule is found to be sputtered from the pure pyridine layer (the D_2O-adsorbed pyridine layer and pyridine-adsorbed D_2O layer) since the proton (deuteron) transfer reactions are induced in the C−H···N (O−D···N) contact during energetic molecular collisions. The pyridine molecule undergoes hydrophilic hydration on the D_2O layer for $T > 100$ K, but no indication of the hydrophobic hydration is observed except for the temperature regime around 150 K, where the mobile D_2O molecules tend to cover the pyridine molecules. On the pyridine layer, the adsorbed D_2O molecules form not only the O−D···N hydrogen bonds with pyridine but also the O−D···O hydrogen bonds in the D_2O island. The latter disappears above 115 K due to the incorporation in the pyridine layer. The benzene molecule dissolves in the D_2O layer considerably for $T > 120$ K due to the occurrence of the hydrophobic hydration, but the D_2O molecule is not incorporated in the C_6H_6 layer. From the comparison of the hydration modes between the pyridine and benzene molecules, it is found that the hydrophobic hydration competes with the hydrophilic hydration because the water-structure formation around the hydrophobic group is disturbed if the hydrogen bond is formed. This is characteristic of the amphiphilic molecules adsorbed on the water-ice surface, where the molecules can be stabilized by pointing the hydrophobic end group toward the vacuum side.

References and Notes

(1) Feller, D. *J. Phys. Chem. A* **1999**, *103*, 7558.
(2) Garrett, A. W.; Zwier, T. S. *J. Chem. Phys*. **1992**, *96*, 3402.
(3) Pribble, R. N.; Zwier, T. S. *Science* **1994**, *265*, 75.
(4) Gruenloh, C. J.; Carney, J. R.; Arrington, C. A.; Zwier, T. S.; Fredericks, S. Y.; Jordan, K. D. *Science* **1997**, *276*, 1678.
(5) Gotch, A. J.; Zwier, T. S. *J. Chem. Phys*. **1992**, *96*, 3388.
(6) Devlin, J. P.; Buch, V. *J. Phys. Chem*. **1995**, *99*, 16534.
(7) Gunster, J.; Liu, G.; Stultz, J.; Krischok, S.; Goodman, D. W. *J. Phys. Chem. B* **2000**, *104*, 5738.
(8) Souda, R. *J. Chem. Phys*. **2003**, *119*, 2774.
(9) Souda, R.; Kawanowa, H.; Kondo, M.; Gotoh, Y. *J. Chem. Phys*. **2003**, *119*, 6194.
(10) Lancaster, G. M.; Honda, F.; Fukuda, Y.; Rabalais, J. W. *J. Am. Chem. Soc*. **1979**, *101*, 1951.
(11) Magnera, T. F.; David, D. E.; Stulik, D.; Orth, R. G.; Jonkman, H. T.; Michl, J. *J. Am. Chem. Soc*. **1989**, *111*, 5036.
(12) Kang, H.; Shin, T.-H.; Park, S.-C.; Kim, I. K.; Han, S.-J. *J. Am. Chem. Soc*. **2000**, *122*, 9842.
(13) Stevenson, K. P.; Kimmel, G. A.; Dohnalek, Z.; Smith, R. S.; Kay, B. D. *Science* **1999**, *283*, 1505.
(14) Gu, Y.; Kar, T.; Scheiner, S. *J. Am. Chem. Soc*. **1999**, *212*, 9411.
(15) Kryachko, E. S.; Zeegers-Huykens, T. *J. Phys. Chem. A* **2001**, *105*, 7118.
(16) Polta, J. A.; Thiel, P. A. *J. Am. Chem. Soc*. **1986**, *108*, 7560.
(17) Jakob, P.; Menzel, D. *Surf. Sci*. **1989**, *220*, 70.
(18) Gunster, J.; Stultz, J.; Krischok, S.; Goodman, D. W. *Chem. Phys. Lett*. **1999**, *306*, 335.
(19) Blanchard, J. L.; Roberts, J. T. *Langmuir* **1994**, *10*, 3303.
(20) Livneh, T.; Romn, L.; Asscher, M. *Surf. Sci*. **1996**, *351*, 250.
(21) Smith, R. S.; Huang, C.; Wong, E. K. L.; Kay, B. D. *Phys. Rev. Lett*. **1997**, *79*, 909.
(22) Souda, R. *J. Chem. Phys*. **2002**, *116*, 8556.
(23) Kawanowa, H.; Kondo, M.; Gotoh, Y.; Souda, R. To be published.
(24) Marsh, A. L.; Gland, J. L. *Surf. Sci*. **2003**, *536*, 145.
(25) Litorja, M.; Haynes, C. L.; Haes, A. J.; Jensen, T. R.; Van Duyne, R. P. *J. Phys. Chem. B* **2001**, *105*, 6907.
(26) Taylor, R.; Kennard, O. *J. Am. Chem. Soc*. **1982**, *104*, 5063.
(27) Steiner, T.; Saenger, W. *J. Am. Chem. Soc*. **1992**, *114*, 10146.
(28) Steiner, T.; Saenger, W. *J. Am. Chem. Soc*. **1993**, *115*, 4540.
(29) Novoa, J. J.; Tarron, B.; Whangbo, M.-H.; Williams, J. M. *J. Chem. Phys*. **1991**, *95*, 5179.
(30) Szczesniak, M. M.; Chalasinski, G.; Cybulski, S. M.; Cieplak, P. *J. Chem. Phys*. **1993**, *98*, 3078.
(31) Alkorta, I.; Maluendes, S. *J. Phys. Chem*. **1995**, *99*, 6457.
(32) Allerhand, A.; Schleyer, P. v. R. *J. Am. Chem. Soc*. **1963**, *85*, 1715.
(33) Novoa, J. J.; Tarron, B.; Whangbo, M. H.; Williams, J. M. *J. Chem. Phys*. **1991**, *95*, 5179.
(34) Materer, N.; Starke, U.; Barbieri, A.; van Hove, M. A.; Somorjai, G. A.; Kroes, G. J.; Minot, C. *Surf. Sci*. **1997**, *381*, 190.
(35) Glebov, A.; Graham, A. P.; Menzel, A.; Toennies, J. P.; Senet, P. *J. Chem. Phys*. **2000**, *112*, 11011.
(36) Bertie, J. E.; Devlin, J. P. *J. Chem. Phys*. **1983**, *78*, 6203.
(37) Collier, W. B.; Ritzhaupt, G.; Devlin, J. P. *J. Phys. Chem*. **1984**, *88*, 363.
(38) Wooldridge, P. J.; Devlin, J. P. *J. Chem. Phys*. **1988**, *88*, 3086.
(39) Wei, X.; Miranda, P. B.; Shen, Y. R. *Phys. Rev. Lett*. **2001**, *86*, 1554.
(40) Smith, R. S.; Huang, C.; Kay, B. D. *J. Phys. Chem*. B **1997**, *101*, 6123.
(41) Smith, R. S.; Kay, B. D. *Nature* **1999**, *398*, 788.
(42) Jenniskens, P.; Banham, S. F.; Blake, D. F.; McCoustra, M. R. S. *J. Chem. Phys*. **1997**, *107*, 1232.